ACI MATERIALS JOURNAL TECHNICAL PAPER

Title no. 108-M16

Space-Averaged Constitutive Model for HPFRCCs with Multi-Directional Cracking

by Kohei Nagai, Benny Suryanto, and Koichi Maekawa

This paper focuses on the numerical modeling of high-performance fiber-reinforced cementitious composites (HPFRCCs), specifically polyvinyl alcohol engineered cement composites (PVA-ECCs) in the context of a space-averaged, fixed-crack approach. Compression, tension, and shear models are proposed. The compression and tension models include internal unloading and reloading paths. The shear model considers the shear stress transfer contributed by surface friction and fiber bridging in a phenomenological manner. The applicability of the models is verified against recent experiments on precracked PVA-ECC plates subjected to principal stress rotation, demonstrating that the proposed models replicate various responses of the plates. The degradation of initial stiffness and the overall strength of plates with precracks at different angles is represented well. Finally, this paper demonstrates the ability of the models to replicate the average strains spanning bidirectional multiple cracks occurring at the bottom surface of the precracked plates.

Keywords: high-performance fiber-reinforced cementitious composite; multi-directional cracking; polyvinyl alcohol engineered cement composite; shear transfer; space-averaged model.

INTRODUCTION

High-performance fiber-reinforced cementitious composites (HPFRCCs) are one type of fiber-reinforced cementitious composites (FRCCs)[1] that exhibit multiple cracking and pseudo-strain-hardening behavior under tension. The engineered cementitious composites (ECCs) that have been introduced since the 1990s are one example of an HPFRCC. Typically, ECCs contain fine-graded aggregate particles and a moderate amount of short, random fibers (approximately 2 to 3%). Different fiber types have been used to produce ECCs, including steel,[2] polyethylene (PE), and polyvinyl alcohol (PVA) fibers.[3] Types of ECCs containing PVA fibers have been recently used in several full-scale applications.[4]

In using these materials in general applications, a complete understanding of their post-cracking behavior when subjected to general loading conditions is necessary. For example, consider a bridge deck made of ECC. Due to the random movement of wheels over the deck, cracks can first occur at different locations on the deck. Once formed, these cracks can alternately open and close as well as simultaneously slip, allowing not only tensile stresses to develop at cracks, but also shear stresses.

Although a great deal of effort has been made to investigate the tensile behavior of ECCs, considerably less effort has been made regarding the issue of crack-shear transfer in ECCs. To obtain insight into this issue, the authors recently conducted experimental investigations on the behavior of precracked PVA-ECC plates subjected to principal stress rotation.[5] The experimental results showed that the cracks exhibited an orthogonal pattern. This might be attributed to a lack of interface shear transfer, likely occurring due to the absence of coarse aggregates. To substantiate this finding, the results of the earlier experiments are reviewed in this paper from an analytical perspective.

Several numerical analysis approaches have been proposed for the behavior of ECCs. Kabele[6-8] provides a multi-scale framework that can relate the behavior of a single fiber to the behavior of the structural element. This framework, which is based on a fixed-crack approach, has been shown to be applicable in various cases. The cracked ECC is treated as a material that can transfer stresses normal and parallel to cracks, as well as transfer shear across the cracks. Suwada and Fukuyama[9] show that the behavior of shear-critical reinforced HPFRCC members can be adequately predicted once the appropriate postcracking biaxial tension-compression behavior of the material is known. In this case, the analysis was performed based on a rotating crack approach, so no shear modeling was proposed.

In this paper, an attempt is made to develop space-averaged constitutive models of PVA-ECCs that will be useful in performing simulations of ECCs with bidirectional cracking as a result of complex stress conditions. Three constitutive models are considered: compression, tension, and shear. Particular attention is paid to the shear model because it has been overlooked thus far. In pursuing this analysis, use is made of the results obtained in the authors' recent experimental investigation.

RESEARCH SIGNIFICANCE

This paper focuses on numerical modeling of PVA-ECCs. Particular attention is paid to the modeling of shear transfer, which has been overlooked thus far. The modeling of shear transfer is considered important to analytical simulations in the case that the material is subjected to general loading conditions. Along with the compression and tension models, the shear transfer model is verified against experiments on precracked PVA-ECC plates that undergo principal stress rotation. In general, the behavior seen in the experiments is simulated fairly well by the models. The hope herein is that the models can be used to perform structure-scale simulations that expand the applicable range of PVA-ECCs.

SUMMARY OF EXPERIMENTAL PROGRAM: ECCs WITH MULTI-DIRECTIONAL CRACKING

An experimental program to investigate the behavior of precracked PVA-ECC plates subjected to principal stress

ACI Materials Journal, V. 108, No. 2, March-April 2011.
MS No. M-2009-271.R4 received May 31, 2010, and reviewed under Institute publication policies. Pertinent discussion including authors' closure, if any, will be published in the January-February 2012 *ACI Materials Journal* if the discussion is received by October 1, 2011.

Kohei Nagai *is an Assistant Professor in the Department of Civil Engineering at the University of Tokyo, Tokyo, Japan. He received his DEng in engineering from Hokkaido University, Hokkaido, Japan, in 2005. His research interests include the nonlinear mechanics of fiber-reinforced and reinforced concrete and the mesoscale discrete analysis of cementitious materials.*

Benny Suryanto *is a Post-Doctoral Fellow in the Department of Civil Engineering at the University of Tokyo. He received his PhD from the University of Tokyo in 2009. His research interests include the nonlinear mechanics of fiber-reinforced and reinforced concrete.*

ACI member **Koichi Maekawa** *is a Professor in the Department of Civil Engineering at the University of Tokyo. He received his DEng in engineering from the University of Tokyo in 1985. His research interests include the nonlinear mechanics of reinforced concrete, performance-based evaluation and life-span simulation of reinforced concrete structures, soil-structure interaction, and multi-scale analysis of cementitious materials.*

rotation was recently conducted by the authors.[5] A summary of the experiment is shown in Table 1 and the results are briefly described herein. Also included in this paper are the results of a recent experiment in which the effects of transverse cracking were investigated (Specimens S13 through S18 in Table 1).

Material and experimental parameters

The ECC investigated in the study is a premix type available in Japan. It contains PVA fibers that are 12 mm (0.47 in.) in length in the proportion of 2% by volume. Details of the mixture proportion and the fabrication guidelines can be found in the Japan Society of Civil Engineers (JSCE) recommendations.[10] Eighteen plate specimens were produced in three batches. The dimensions of the specimens and the experimental parameters are given in Fig. 1 and Table 1. Basically, two types of specimens were used. The first is designated as the control specimen (Specimens S1, S2, S9, and S10) and has dimensions of 400 x 250 x 20 mm (16 x 10 x 0.79 in.), and the second type of specimen is designated as the main specimen (Specimens S3 through S8, S11, and S14) and has dimensions of 550 x 420 x 20 mm (22 x 17 x 0.79 in.). Two experimental parameters are considered, as shown in Table 1: the first is the orientation of the initial crack (20, 45, 70, and 90 degrees), while the second is the degree of initial damage. The degrees of damage considered correspond to 40 and 70% of the average ultimate tensile strains of the control plates. The tensile strain was measured from the bottom surface of each plate. For the third batch (Specimens S13 through S18), additional initial damage degrees at a crack orientation of 90 degrees were considered so as to examine the effects of transverse cracking on plate behavior.

Testing procedure

Figure 2 shows the testing procedure adopted in the experiment. For the control specimens, a four-point bending test was performed. For the main specimens, initial cracks were first introduced by performing a bending test (A). Unloading took place when the initial strain reached a specified value of 40 or 70% of ε_{tu}. After unloading, reversed loading (C) was applied to flatten the specimen (D). The specimen was then cut as shown in Fig. 2 (E). This process altered the orientation of the initial crack to a certain angle relative to the longitudinal axis of the specimen. Finally, the cut specimen was retested in a four-point bending procedure (G).

Measurements

Two types of transducers were used: linear variable differential transducers (LVDTs) and miniature cable position transducers (CPTs). The LVDTs were used to measure the midspan deflection of the plates, whereas the CPTs measured average strains occurring at the bottom surface of the plate spanning several cracks (refer to Fig. 3). These average strain values will be compared with the computed strains obtained from analysis later in this paper.

Results of experiment

Figure 4 shows the load versus midspan deflection relationship for the control and main Specimens S1 through S12 at point (G) in Fig. 2. (Note that in the experiment,

Table 1—Experimental program

Batch	Plate ID	Dimensions			Initial damage		Plate type	Initial crack angle in experiment, degree
		W, mm	L, mm	H, mm	Orientation, degree	Degree, % of ε_{tu}		
1	S1	400	250	20	—	—	Control	—
	S2	400	250	20	—	—	Control	—
	S3	550	420	20	20	40	Main	24
	S4	550	420	20	20	70	Main	21
	S5	550	420	20	45	40	Main	44
	S6	550	420	20	45	70	Main	35
	S7	550	420	20	70	40	Main	63
	S8	550	420	20	70	70	Main	68
2	S9	400	250	20	—	—	Control	—
	S10	400	250	20	—	—	Control	—
	S11	550	420	20	90	40	Main	—
	S12	550	420	20	90	70	Main	—
3	S13	400	250	20	—	—	Control	—
	S14	400	250	20	—	—	Control	—
	S15	550	420	20	90	10	Main	—
	S16	550	420	20	90	15	Main	—
	S17	550	420	20	90	40	Main	—
	S18	550	420	20	90	90	Main	—

Notes: Control specimen is 400 x 250 x 20 mm (16 x 10 x 0.79 in.); main specimen is 550 x 420 x 20 mm (20 x 17 x 0.79 in.); 1 mm = 0.039 in.

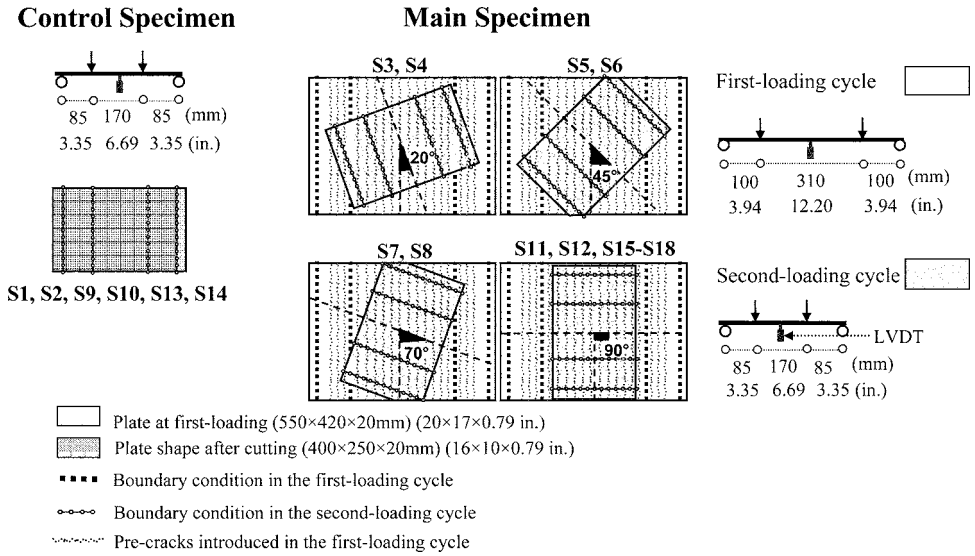

Fig. 1—Layout of specimens in experiment.

Specimen S4 started from a nonzero displacement due to the accidental contact between the loading head and the top of the specimen prior to loading commencement. The result is still kept because the load and strains were properly measured.) All specimens showed a ductile response. Compared to the response of the control specimens, main Specimens S3 to S8 indicated that the initial damage had a significant influence, particularly on the strength and initial stiffness. Figure 5 summarizes the reduction ratio of initial stiffness and strength of each main specimen with respect to the average angle of the precracks measured at the bottom of each specimen. The reduction ratios shown were obtained by normalizing the values obtained from each specimen to those obtained from the control specimens. Also shown in the figure are the results obtained by analysis, which will be discussed in a later part of this paper. The reduction in strength tends to increase with increasing initial crack orientation until the orientation of the initial crack approaches 90 degrees and then begins to decrease. The initial stiffness, on the other hand, rises with increasing initial crack orientation up to 90 degrees.

The cracking patterns of the control specimens (Specimens S1 and S9) and main specimens (Specimens S3 to S8 and S15 to S16) after failure are shown in Fig. 6. The control specimens, which were subjected to a fixed stress direction, show cracks that are approximately parallel to each other. The main specimens, on the other hand, show a somewhat orthogonal crack pattern consisting of precracks and secondary cracks. The initiation of secondary cracks was predicted by observing the strain parallel to the precracks, as discussed in more detail in the companion paper by the authors.[5] The precracks formed orthogonal to the first principal tensile stress direction, whereas the secondary cracks did not form orthogonal to the second principal tensile stress direction and formed almost orthogonal to the precracks (within a 15-degree range). In Specimens S3 to S8 (with a 20, 45, and 70-degree precrack orientation), the orthogonal crack pattern suggests that significant anisotropy is exhibited because of inadequate stress transfer along the precracks. Specimens S15 to S18 (with a 90-degree precrack orientation) showed an orthogonal crack pattern. In these specimens, the precracks were approximately along the

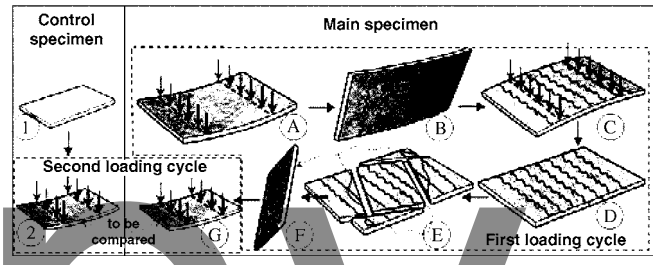

Fig. 2—Testing procedure in experiment.

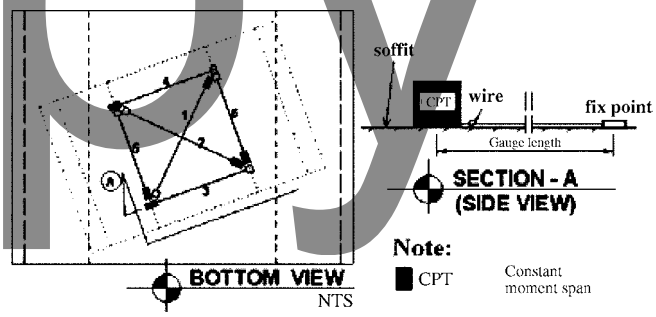

Fig. 3—Deformation measurement device.

longitudinal axis of the specimen. Hence, less significant stresses were induced along the precracks and an orthogonal pattern resulted.

Overall, the experimental results indicate that precracking and stress rotation affect the strength, stiffness, and cracking pattern of the plates. This is due to the fact that the response of the test plates shown is governed by the tensile and shear stresses transferred along the bidirectional cracks. Proper modeling of tensile and shear stresses is therefore essential to accurately predict plate behavior.

SPACE-AVERAGED CONSTITUTIVE MODEL

Three space-averaged constitutive models suitable for PVA-ECCs are proposed. The basic analysis platform is COM3, a three-dimensional nonlinear finite element

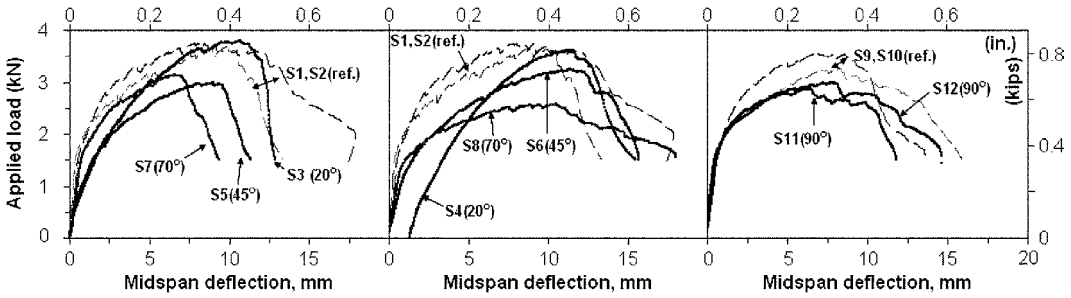

Fig. 4—Load-deflection curve for second loading cycle in experiment.

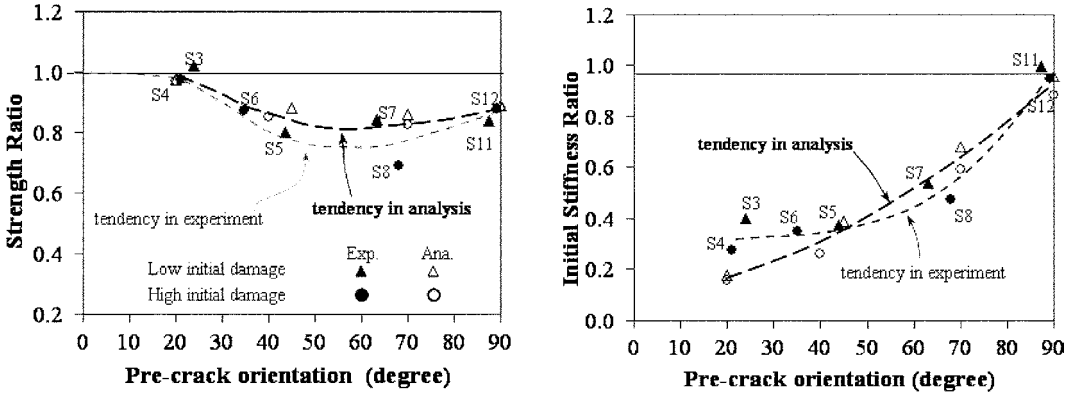

Fig. 5—Strength and stiffness reduction ratio.

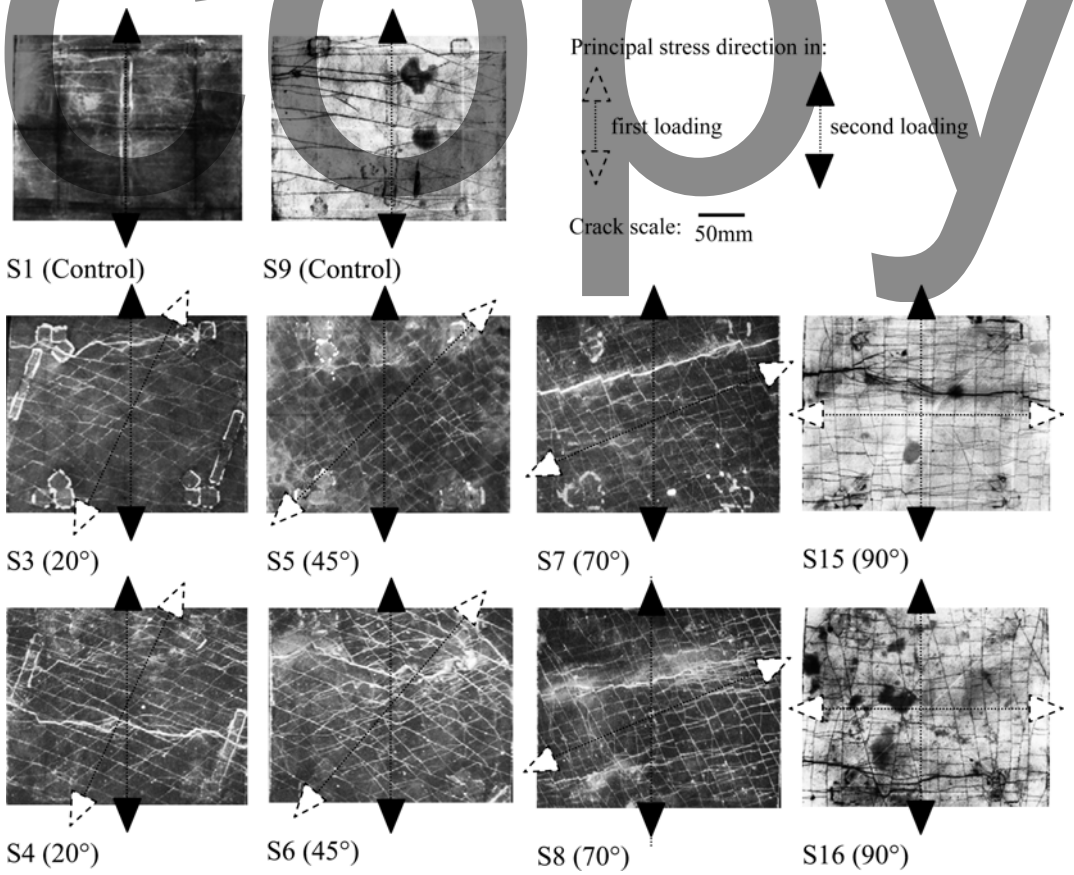

Fig. 6—Crack patterns in experiment. (Note: 1 mm = 0.039 in.)

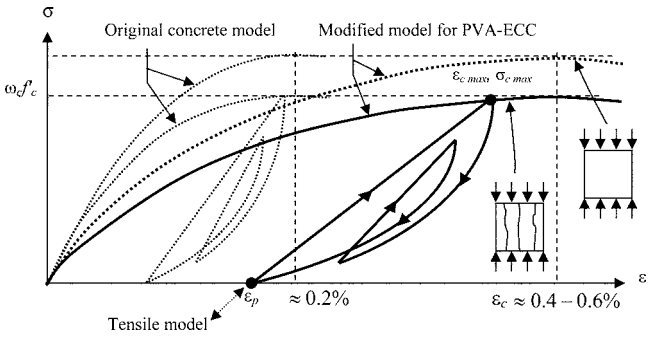

Fig. 7—Uniaxial compression model.

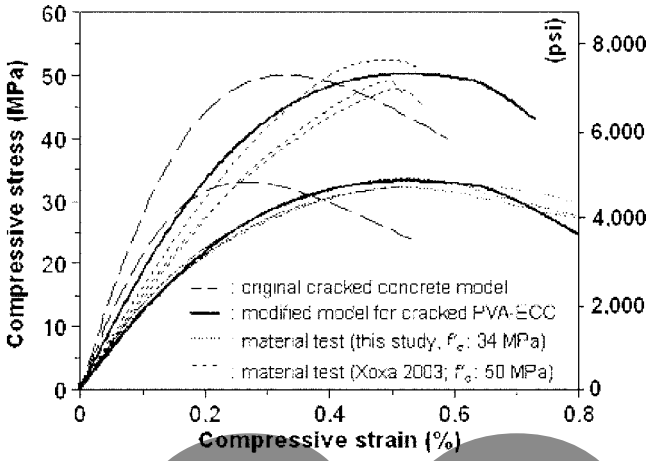

Fig. 8—Verification of compression for PVA-ECC.

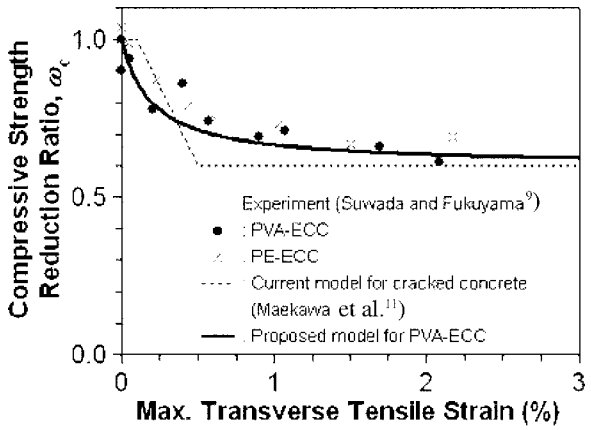

Fig. 9—Compressive strength reduction factor.

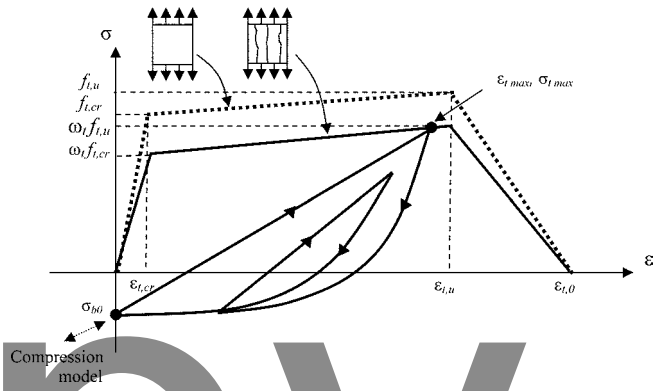

Fig. 10—Uniaxial tensile model.

analysis program for reinforced concrete structures.[11] This platform is based on a space-averaged, fixed-crack approach and the active crack concept. In the platform, three constitutive models of cracked concrete (compression, tension, and shear transfer) and one model of reinforcement are considered to represent the behavior of reinforced concrete element subjected to arbitrary stress conditions and under multi-directional cracking. For the purpose of performing a simulation of cracked PVA-ECC plates, the existing constitutive models of concrete were modified.

Compression model

For this study, the original cracked-concrete model is directly adopted with only a slight modification. The modification was made only in defining the strain at compressive strength ε_c. Herein, the ε_c value is set according to the strain value obtained from material tests (it typically lies in the range of 0.4 to 0.6%). A comparison of the original cracked-concrete compression model[11] and the proposed cracked PVA-ECC compression model is shown in Fig. 7. The postpeak behavior is not discussed in this study.

The verification of the backbone curve of the compression model (without transverse cracking) is shown in Fig. 8. As can be seen in the figure, the proposed model provides essentially the same response for PVA-ECCs with a compressive strength of 34 MPa (4931 psi) as found in the experimental investigation. For PVA-ECCs with a compressive strength of approximately 50 MPa (7251 psi),[12] the proposed model slightly overestimates the initial stiffness.

It has been recognized that as a result of transverse cracking, cracked concrete exhibits a softening phenomenon.[13] A similar phenomenon is assumed to happen in cracked PVA-ECC as well. To include the effects of transverse cracking, the experimental data reported by Suwada and Fukuyama[9] are referenced and shown in Fig. 9. The following expression is thus proposed to include these effects

$$\omega_c = 1 - \left(\frac{2\varepsilon_{tmax}}{1 + 5\varepsilon_{tmax}}\right) \quad (1)$$

where ω_c is the compressive strength reduction factor, and ε_{tmax} is the maximum tensile strain normal to the cracks, defined in percent.

Tensile model

Kanda[14] proposed that the response of PVA-ECCs in tension can be approximately modeled—for the postcracking region up to the peak tensile stress—by a bilinear stress-strain relationship. In this study, this type of treatment is adopted. For the post-peak response, a linear stress-strain relation to zero stress is assumed. The backbone of the tensile model can be seen in Fig. 10.

The unloading-reloading path of the tensile model is assumed to resemble that of the tensile concrete model installed in COM3, with a curved unloading path and a linear reloading path (Fig. 10). Experimental evidence reported by Kesner et al.[15] suggests that the response of PVA-ECCs also has a similar shape, although a different reloading path has also been reported.[16] From tension to compression, the tensile stress is assumed not to return to zero stress, but to a

fictitious stress σ_{b0}. This fictitious stress is assumed so as to account for a kind of premature recontact of crack surfaces due to the ability of fiber bridging to sustain compression stress. The resulting full path of the PVA-ECC tensile model can be seen in Fig. 10.

To account for the effect of transverse cracking, the results of Specimen Plates S9 to S18 are considered and shown in Fig. 11. No substantial strength reduction phenomenon is observed. Based on this finding, the following expression is proposed to account for the effects of transverse cracking on the tensile model

$$\omega_t = 1 - \left(\frac{200\varepsilon_{tmax}^{\ 3}}{1 + 2000\varepsilon_{tmax}^{\ 3}} \right) \tag{2}$$

where ω_t is the strength reduction factor in tension.

Shear model

The shear model considers the contribution of crack friction and fiber bridging. Since PVA-ECCs do not contain coarse aggregates, it is expected that less crack interlocking will occur because the crack surface is flat. It is also assumed that the contribution of PVA fibers in transferring shear stress at the crack is not significant as compared to the effect of aggregate interlocking in concrete. Because the current shear model installed in COM3 is applicable only to concrete with a rough crack surface,[11] a reduction coefficient *A* is introduced. As a result, the proposal is for the following expression

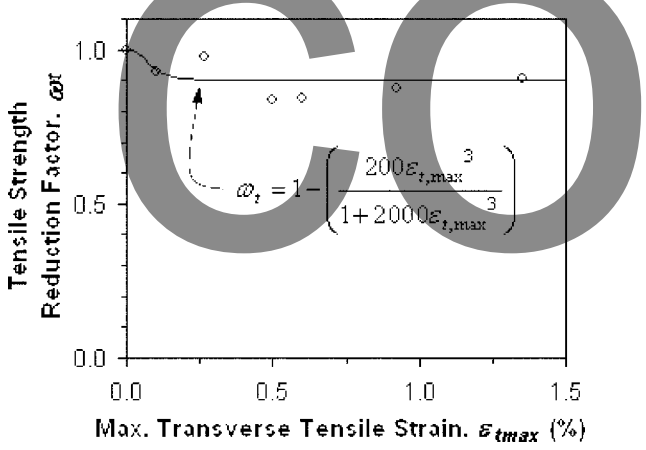

Fig. 11—Tensile strength reduction factor.

$$\tau_{st} = Af_{st}\frac{\beta^2}{1+\beta^2} \tag{3}$$
$$f_{st} = 3.8f_c'^{1/3} \quad \text{(in MPa)}$$

where τ_{st} is the average shear stress, *A* is a new reduction factor to account for the difference in shear capacity between a rough crack surface and a flat crack surface with fiber, and β is the ratio of shear to normal strain. The variable f_{st} is the shear transfer strength, which is a function of compressive strength f_c'. For PVA-ECCs containing 2% fibers by volume, *A* is assumed to be 0.25.

Furthermore, it is proposed that the contribution of the PVA fibers in shear becomes dominant at larger shear deformations, whereas that of shear friction becomes less. This is treated as a shear softening phenomenon. To take it into account, the equation previously used by An[17] for concrete is adopted and is shown in the following (Fig. 12)

$$\tau_{st} = G\gamma \qquad \text{for } \gamma < \gamma_u \tag{4}$$

$$\tau_{st} = G\gamma\left(\frac{\gamma_u}{\gamma}\right)^c \qquad \text{for } \gamma \geq \gamma_u \tag{5}$$

where *G* is the average shear stiffness of cracked PVA-ECC, γ_u is the average shear strain from where the shear softening starts, and *c* is the shear softening coefficient. In the formulation, attention must be paid to defining γ_u and *c*, as these two parameters could be affected by fiber volume. Through parametric analysis,[18] γ_u and *c* are assumed to be 1000 μ and 0.4, respectively. It should be noted herein that the proposed shear model is for use without reinforcement.

NUMERICAL SIMULATION

Model mesh and analysis procedure

To verify the proposed models, the control and main specimens (Specimens S1 to S12) are subjected to analysis. The specimens are modeled using eight-node Mindlin plate elements. Each plate element is divided into nine layers over its depth, each with an independent stress-strain behavior. Due to the complexity of mesh geometry, the width of Specimens S5, S6, S11, and S12 during initial loading is altered in the simulation process, as shown in Fig. 13. (Note that the moment spans are kept similar, so this change has no effect.) The mesh for Specimen S6 is set at 40 degrees

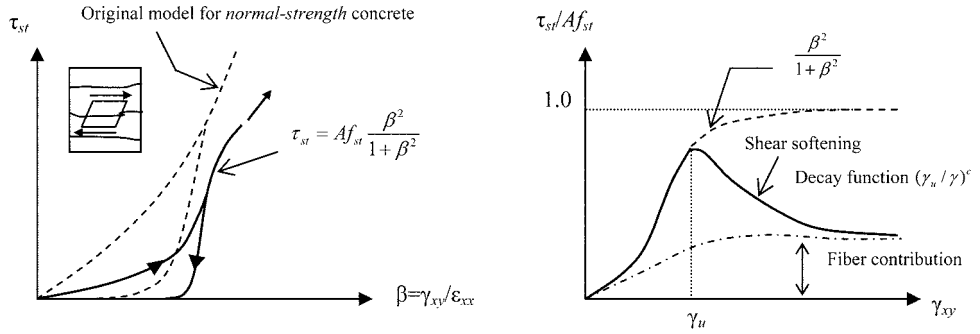

Fig. 12—Average shear stress-strain model of cracked PVA-ECC.

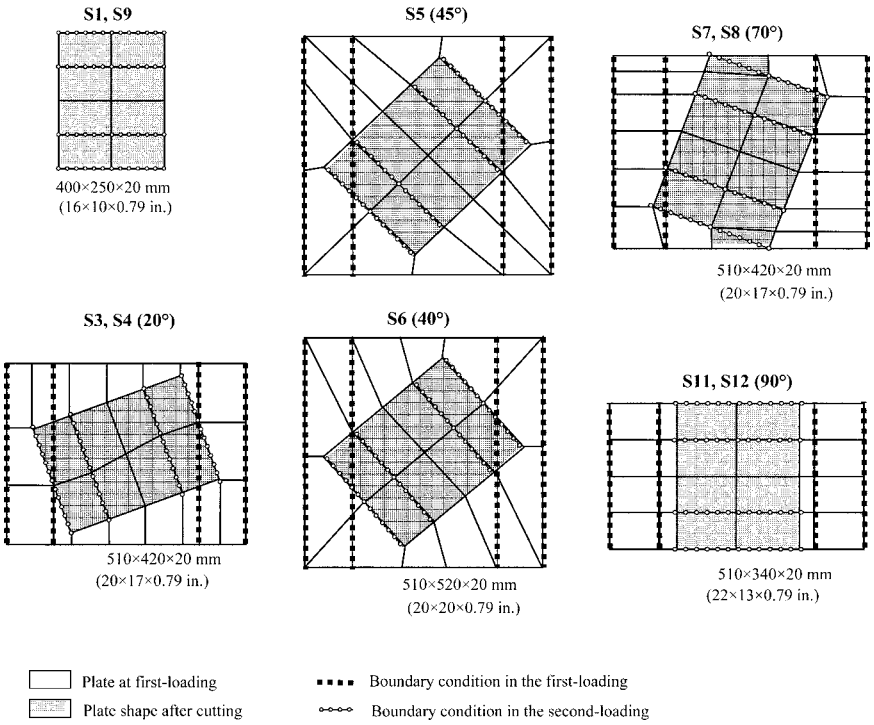

Fig. 13—Mesh arrangement adopted in analysis.

instead of 45 degrees, following the experimentally obtained average precrack angle (refer to Table 1).

Analysis was carried out in a similar manner to the testing procedure adopted in the actual experiment. First, the specimen models were precracked in bending. Reversed bending was then applied to eliminate the residual midspan displacement. After this initial loading, the locations of all support and loading points were updated based on the layout shown in Fig. 13. The elements not used in the analysis of subsequent loading (all the unhatched elements in Fig. 13) were virtually removed from the model by making their stiffness very low. The reaction forces at the previous boundary condition were also released. This complicated analysis procedure can be handled without difficulty by the use of the restart function provided in COM3.

Material properties and analysis of simple bending test

To obtain the material properties of PVA-ECCs for use in the analysis, cylindrical specimens were subjected to compressive tests and control specimens were subjected to bending tests. Tensile properties were determined such that they fitted the results obtained for the control specimens. The resulting material properties are listed in Table 2. The analysis of main Specimens S3 to S8 and S11 to S12 is discussed on the basis of these properties.

First of all, sensitivity analysis was conducted to confirm the suitable number of layers (from three up to the maximum of nine). The outcome of this analysis is shown in Fig. 14, demonstrating that with anything over six layers, there is almost no difference in the analytical results. Because the analysis was to be carried out for precracked plates, a nine-layer model was selected for use throughout the analysis so as to obtain smoother stress and strain profiles along the depth of the plate, thereby ensuring better accuracy.

Table 2—Input material properties

Material property	S1 to S8	S9 to S12
$f_{t,u}$, MPa (psi)	4.0 (580)	3.8 (550)
$f_{t,cr}$, MPa (psi)	2.8 (406)	2.7 (390)
$\varepsilon_{t,u}$	1.25%	1.05%
$\varepsilon_{t,0}$	2.25%	2.25%
f_c', MPa (psi)	33 (4785)	26 (3770)
ε_c	0.50%	0.50%
Poisson's ratio	0.23	0.23

Verification of internal curve

To verify the unloading and reloading model adopted, a reversed bending test on one additional PVA-ECC plate was carried out. This is important because the model will be used to simulate the damage of the tested precrack specimens during the first loading cycle. This verification is also important to ensure that the model is capable of replicating the reopening behavior of the precracks during the second loading. Once this opening-and-closing behavior is adequately simulated, the cracks' behavior in shear during the second loading cycle can be exclusively studied.

To focus on the reloading shape of the tensile model, two different shapes were applied: one with a linear shape, as proposed, and the other using a curve, as shown in Fig. 15(a). The initial cracking stress, ultimate tensile strength, and ultimate tensile strain were assumed as 3.0 MPa (435 psi), 3.4 MPa (493 psi), and 0.75%, respectively. Figure 15(b) compares the simulation with the experimental observations, demonstrating that the linear reloading shape is more suitable for the PVA-ECC type used herein.

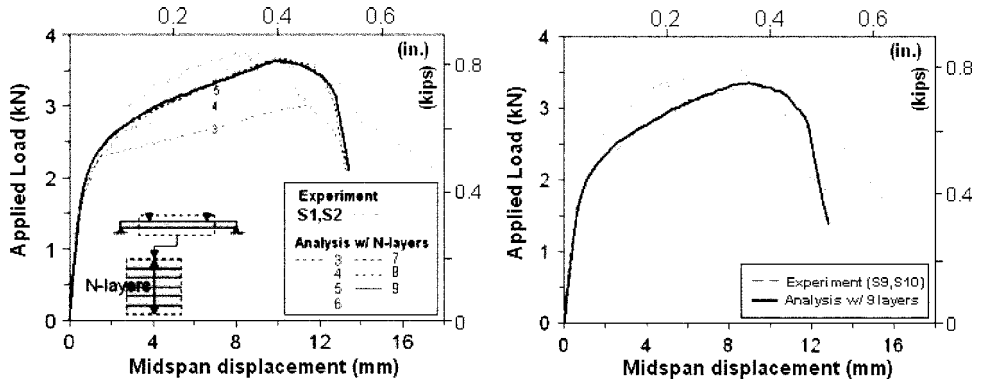

Fig. 14—Analysis of control specimen with different layers.

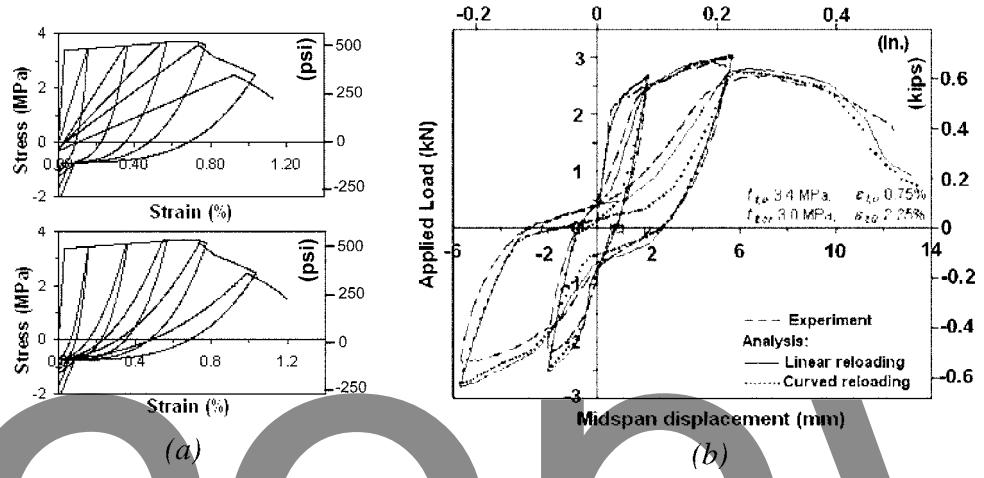

Fig. 15—Tensile model identification: (a) tensile models with two different reloading shapes; and (b) corresponding reversed bending result compared to experiment.

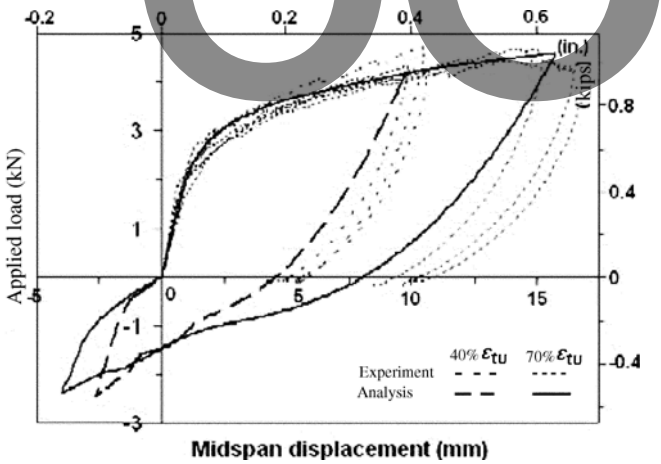

Fig. 16—Load-deflection curves during preloading.

Preloading of main specimens

In the analysis, preloading was applied so as to reflect as closely as possible the preloading in the experiment, thereby ensuring that the plate model would undergo similar damage prior to the second loading. The first loading cycle was applied until the bottom plate strain reached either 0.4 or 0.7 of ε_{tu}, depending on the designated plate. Reversed loading was then applied to completely remove any residual deformation of the plate. A comparison of computed and observed load-deflection responses during the first loading cycle is shown in Fig. 16. In preparation for the second loading cycle, all unnecessary elements were virtually cut away and the boundary conditions were changed (refer to Fig. 13). The plate model was then ready for the second loading. Note that in the second loading cycle, the ECC at each layer of the plate model would be in the reloading path. This also provides a check on the reloading path of the compression and tension models adopted.

Second loading of main specimens

The analytical results for Specimens S3 to S8 in the second loading cycle are presented in Fig. 17, together with the results obtained from the experiment for both the control and main specimens. The first occurrence of a secondary crack is also indicated. As shown, the load-displacement curve during second loading is fairly well simulated by the analytical procedure in terms of various values of initial stiffness, load-deflection shape, and strength degradation. A summary of initial stiffness and strength reduction ratio of the specimens is plotted in Fig. 5. The analytical simulation reproduces the observed reduction ratios quite well.

To verify the proposed material models in more detail, the average strain of the bottom of each plate obtained from the experiment and analysis is compared. For ease of comparison, local x- and y-coordinates are introduced, with the x-direction aligned with the direction of the precrack opening. The observed and computed strains of Specimens S4, S6, and S8 are

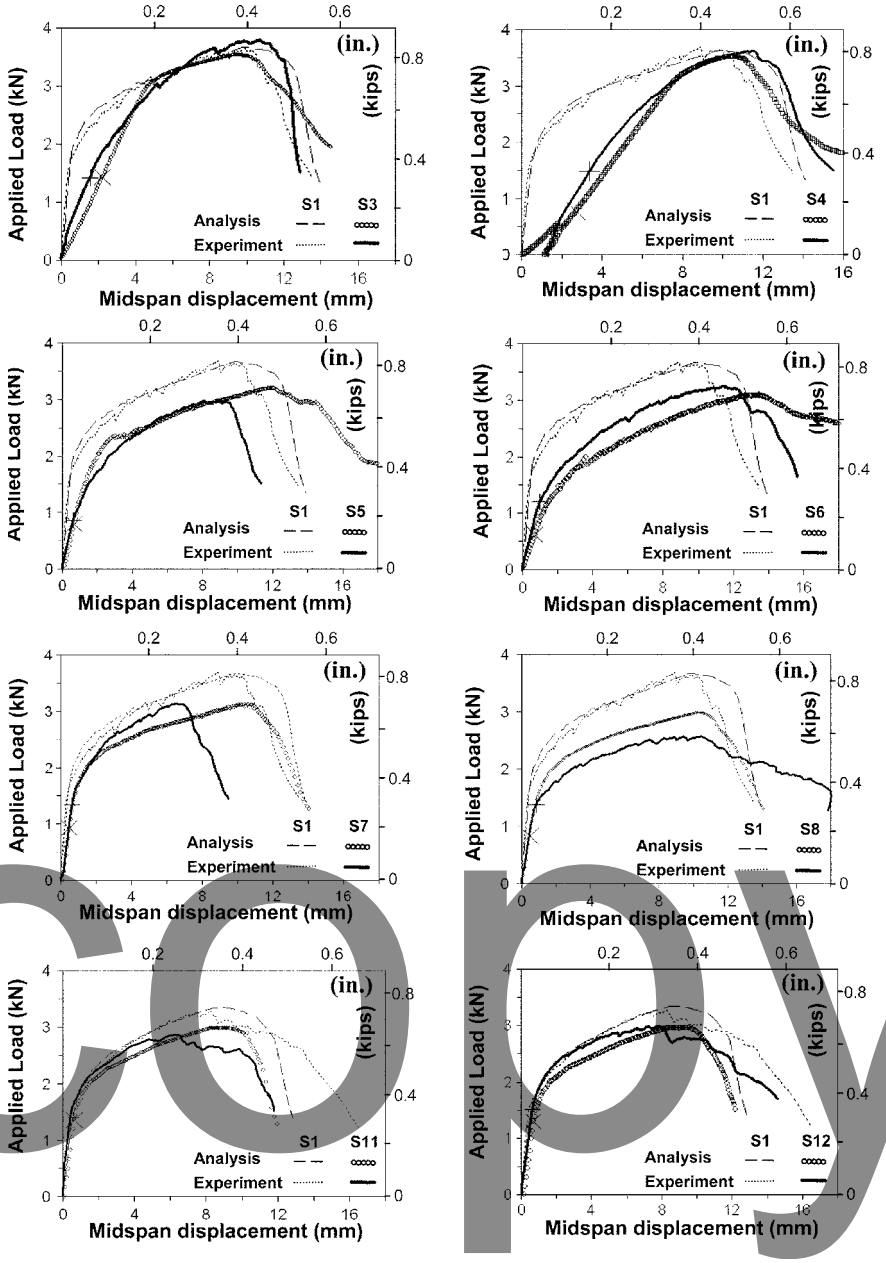

Fig. 17—Load-deflection curves during second loading cycle.

compared in Fig. 18 for specimens with high initial damage and precrack angles of 20, 45, and 70 degrees, respectively. In the case of Specimen S4 (refer to Fig. 18(a), (d), and (g)), the strain normal to the precrack ε_{xx} and shear strain γ_{xy} is much larger than the strain parallel to the precrack ε_{yy}. This means that the significant reduction in initial stiffness in the load-displacement curve shown in Fig. 17 can be attributed to the opening and sliding of the precracks. Ultimately, failure is caused by tensile failure at the precrack.

In contrast to this behavior, the response of Specimen S8—the 70-degree precrack case (refer to Fig. 18(c), (f), and (i))—is dominated by the strain components parallel to the precrack ε_{yy} and shear strain γ_{xy}. The ε_{yy} is dominant, as the orientation of the components parallel to the precracks is close to the new principal stress direction (approximately 20 degrees). At the early loading stage, the ε_{yy} represents the strain of the uncracked part so that it is much stiffer. At this stage, the γ_{xy} values are small due to the limited opening of precracks ε_{xx}. This explains the slight reduction in initial stiffness observed in the load-displacement relationship. In this plate series, the influence of transverse cracking is dominant because the transverse cracks in this case are the precracks that have sustained much larger strain during preloading and causes a reduction in plate strength. In these two specimens (Specimens S4 and S8), the observed and computed shear strains γ_{xy} are comparable.

When the precracks are aligned at 45 degrees, as in Specimen S6, the development of strains in all directions is more significant. That is, whereas the shear strain γ_{xy} (refer to Fig. 18(h)) exhibits the largest value, the other two strains ε_{xx} and ε_{yy} are also significantly high. The larger shear deformation γ_{xy} in particular implies more crack slip due to the large opening of both precracks and secondary cracks (ε_{xx} and ε_{yy}) and less shear transfer resistance along the cracks. Although the effects of transverse cracking are less herein, the inability of the material to transfer shear stress contributes to a greater strength reduction. As a result, the strength reduction ratio becomes comparable to that of Specimen S8.

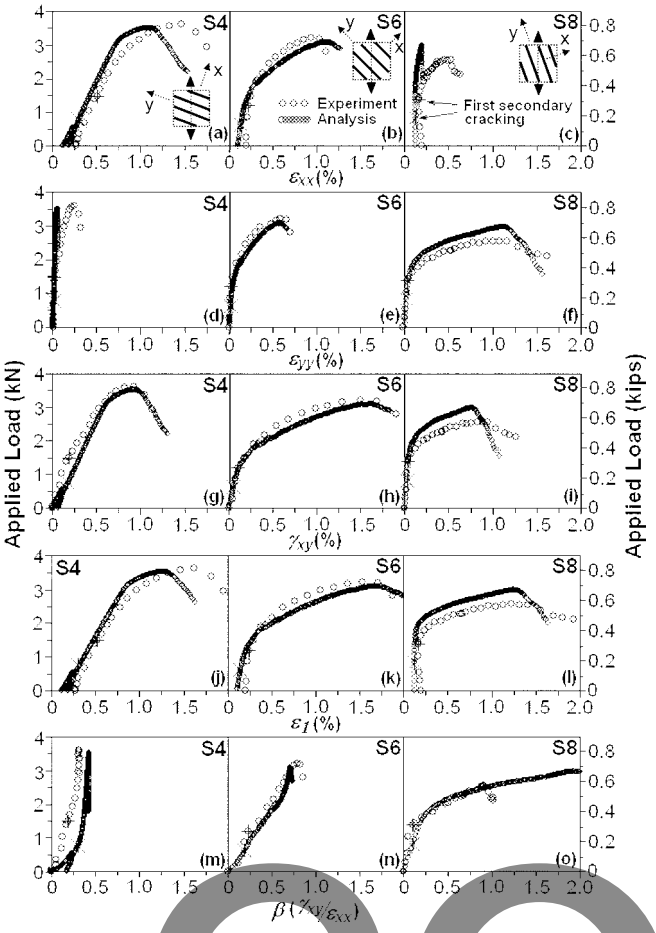

Fig. 18—Bottom face response of Plates S4, S6, and S8.

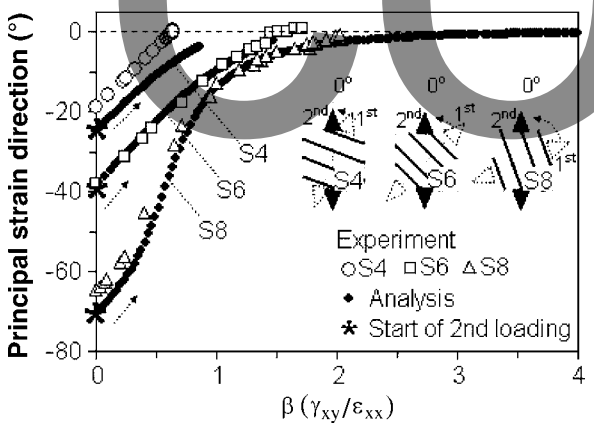

Fig. 19—Principal strain direction.

A comparison of the computed and observed load versus principal tensile strains ε_1 is shown in Fig.18(j) through (l). Both appear in a good agreement and indicate that the three plates undergo significant ε_1 during loading. The source of this significant strain is due to the response of the cracks described in the previous paragraph and shown in Fig. 18(a) through (i). Hence, it appears that the interpretation based on the local x- and y-coordinates is more meaningful.

To obtain the kinematics of the cracks, the value of strain ratio β, which is the ratio of shear-to-normal strain, is shown in Fig. 18(m) through (o) and discussed herein. The β values show a different tendency in the three cases, especially after the secondary crack. With Specimen S4, the value of β stops incrementing after the second crack, which means that the ratio of initial crack opening to shear deformation remains almost constant. In Specimen S6, β increases until approximately 1.5 in both the experiment and analysis. It continues to increase more in Specimen S8, where the shear deformation increases more than the initial crack opening. These behaviors relate to a shift in the principal strain direction. The principal strain direction obtained from the experiment and analysis shows that, at the first stage of the second loading cycle, the principal strain direction does not accord with the principal stress direction, which is along the longitudinal axis of the plate. For clarity, Fig. 19 presents the progress of the principal strain direction as obtained in the experiment and analysis. In all cases, the direction of the principal strain deviates from 0 degrees and the value is approximately comparable to the precrack angle. During loading, the direction of the principal strain gradually shifts toward 0 degrees. As can be observed, β stops growing when the principal strain direction comes close to 0 degrees (refer to Fig. 18(j) through (l)). After this point, all the specimens deform in the direction of the applied stress, which is along the longitudinal axis of the plate.

In all the predictions discussed herein, although the precracked plates have been exposed to a complex stress history, the analysis gives results that are close to the experimental results, covering all initial damage levels and angles tested.

CONCLUSIONS

This study focuses on the numerical modeling of PVA-ECCs based on the space-averaged, fixed-crack approach. Three space-averaged constitutive models are proposed: compression, tension, and shear. The models are completely path-dependent and hence useful to simulate damage in ECCs. The shear model, as proposed, includes shear stress transfer across cracks and the fiber contribution. These models are then installed into the nonlinear analysis framework COM3 for verification. The following conclusions can be derived from this study:

1. The analysis results confirm the applicability of the proposed models. Using these models, the analytical framework is able to simulate the behavior of precracked PVA-ECC plates fairly well, although the plates are first precracked and then subjected to a rotation of the stress field. The ability to successfully replicate the various initial stiffnesses of the plates, in particular, confirms the applicability of the reloading path of the tensile and compression models and the shear model adopted. The distinctive shape of the load-displacement curve during the second loading cycle and the strength degradation ratio are well simulated.

2. Confirming a phenomenon observed in experiments, the tested precracked specimens were highly dependent on the orientation of the precracks. Both the experiment and analysis confirm that the postcracking response of PVA-ECCs in any direction is not equal, but depends on how the stresses are transmitted across the cracks.

3. Both the experiment and analysis confirm that the degree of the anisotropy in cracked ECCs is high due to weak stress transfer at crack locations. In this test series, this high crack-induced anisotropy is marked by the secondary crack that always forms nearly orthogonal to the precrack.

4. The applicability of the proposed models is also confirmed by their ability to trace the values of strains normal and parallel to the precracks and shear strain while subjected to principal stress rotation.

NOTATION

A	=	reduction factor to account for shear capacity of HPFRCC
f_c'	=	uniaxial compressive strength
f_{st}	=	shear transfer strength
$f_{t,cr}$	=	cracking strength
$f_{t,u}$	=	peak tensile stress
G	=	average shear stiffness
β	=	normalized shear strain ($= \gamma_{xy}/\varepsilon_{xx}$)
ε_c	=	strain at peak compressive stress
ε_p	=	plastic strain
$\varepsilon_{t,0}$	=	tensile strain at which tensile stress becomes zero
$\varepsilon_{t,cr}$	=	tensile strain at cracking stress
ε_{tmax}	=	past maximum transverse tensile strain
$\varepsilon_{t,u}$	=	tensile strain at peak tensile stress
ε_{xx}	=	strain normal to crack
ε_{yy}	=	strain parallel to crack
γ_u	=	shear strain from which shear softening starts
γ_{xy}	=	shear strain
σ_{b0}	=	fictitious stress resulting from fiber bridging
$\sigma_{c\,max}'$	=	past maximum compressive stress
$\sigma_{t\,max}$	=	past maximum tensile stress
τ_{st}	=	shear stress
ω_c	=	strength reduction factor in compression
ω_t	=	strength reduction factor in tension

REFERENCES

1. Naaman, A. E., and Reinhardt, H. W., "Characterization of High Performance Fiber Reinforced Cement Composites—HPFRCC," *Proceedings of the Second International RILEM Workshop on High Performance Fiber Reinforced Cement Composite 2 (HPFRCC 2)*, Pro. 31, E&FN Spon, London, UK, 1996.

2. Li, V. C. et al., "Tensile Behavior of Cement Based Composites with Random Discontinuous Steel Fibers," *Journal of the American Ceramics Society*, V. 79, No. 1, 1996, pp. 74-78.

3. Li, V. C.; Wang, S.; and Wu, C., "Tensile Strain-Hardening Behavior of PVA-ECC," *ACI Materials Journal*, V. 98, No. 6, Nov.-Dec. 2001, pp. 483-492.

4. Kunieda, M., and Rokugo, K., "Recent Progress on HPFRCC in Japan," *Journal of Advanced Concrete Technology*, V. 4, No. 1, 2006, pp. 19-33.

5. Suryanto, B.; Nagai, K.; and Maekawa, K., "Bidirectional Multiple Cracking Tests on HPFRCC Plates," *ACI Materials Journal*, V. 107, No. 5, Sept.-Oct. 2010, pp. 450-460.

6. Kabele, P., "Assessment of Structural Performance of Engineered Cementitious Composites by Computer Simulation," *CTU Reports*, V. 5, No. 4, 2001, 99 pp.

7. Kabele, P., "Fracture Behavior of Shear-Critical Reinforced HPFRCC Members," *Proceedings of the International Workshop on HPFRCC in Structural Applications*, HI, May 2005.

8. Kabele, P., "Multiscale Framework for Modeling of Fracture in High Performance Fiber Reinforced Cementitious Composite," *Engineering Fracture Mechanics*, V. 74, No. 1-2, Jan. 2007, pp. 194-209.

9. Suwada, H., and Fukuyama, H., "Nonlinear Finite Element Analysis on Shear Failure of Structural Elements Using High Performance Fiber Reinforced Cement Composite," *Journal of Advanced Concrete Technology*, V. 4, No. 1, 2006, pp. 45-57.

10. JSCE Concrete Library 127, "Recommendations for Design and Construction of High Performance Fiber Reinforced Cement Composite with Multiple Fine Cracks (HPFRCC)," Japan Society of Civil Engineers, 2007, pp. 129-135. (in Japanese)

11. Maekawa, K.; Pimanmas, A.; and Okamura, H., *Nonlinear Mechanics of Reinforced Concrete*, E&FN Spon, London, UK, 2003, 768 pp.

12. Xoxa, V., "Investigating the Shear Characteristics of High Performance Fiber Reinforced Concrete," master's thesis, University of Toronto, Toronto, ON, Canada, 2003.

13. Vecchio, F. J., and Collins, M. P., "The Response of Reinforced Concrete to In-Plane Shear and Normal Stresses," *Publication* No. 82-03, University of Toronto, Toronto, ON, Canada, Mar. 1982.

14. Kanda, T., "Design of Engineered Cementitious Composites for Ductile Seismic Resistant Elements," PhD thesis, University of Michigan, Ann Arbor, MI, May 1998.

15. Kesner, K. E.; Billington, S. L.; and Douglas, K. S., "Cyclic Response of Highly Ductile Cement-Based Composites," *ACI Materials Journal*, V. 100, No. 5, Sept.-Oct. 2003, pp. 381-390.

16. Fukuyama, H., and Suwada, H., "Experimental Response of HPFRCC Dampers for Structural Control," *Journal of Advanced Concrete Technology*, V. 1, No. 3, 2003, pp. 317-326.

17. An, X., "Failure Analysis and Evaluation of Seismic Performance for Reinforced Concrete in Shear," PhD thesis, the University of Tokyo, Tokyo, Japan, 1995.

18. Suryanto, B., "Mechanics of High Performance Fiber Reinforced Cementitious Composite (HPFRCC) under Principal Stress Rotation," PhD thesis, the University of Tokyo, Tokyo, Japan, 2009.